

Petrography of Construction and Demolition Waste (CDW)
from Abruzzo Region (Central Italy)

Galderisi A. ^{*1,2}, Iezzi G. ^{1,3}, Bianchini G. ⁴, Paris E. ⁵ and de Brito J. ⁶

¹ Dipartimento INGEO (Ingegneria & Geologia), Università di Chieti-Pescara ‘G. d’Annunzio’,
Chieti, Italy

² Istituto di Geologia Ambientale e Geoingegneria IGAG - Centro Nazionale delle Ricerche CNR
Rome, Italy

³ Istituto Nazionale di Geofisica e Vulcanologia INGV, Rome, Italy

⁴ Dipartimento di Fisica e Scienze della Terra, Università di Ferrara, Ferrara, Italy

⁵ Scuola di Scienze e Tecnologie, sez. Geologia, Università di Camerino, Camerino, Italy

⁶ CERIS, Instituto Superior Técnico, Universidade de Lisboa, Lisboa, Portugal.

*corresponding author: antonio.galderisi@unich.it, g.iezzi@unich.it

Keywords: CDW (construction and demolition waste), Abruzzo region (Italy), XRPD, XRF, recycling.

Abstract

The density, colour and texture, plus mineral and chemical features of 18 ceramic-like CDW samples from the Abruzzo region (Central Italy) were characterised. The concretes, natural stones, tiles, roof-tiles, bricks and perforated bricks are either aphanitic to porphyric. Concretes and natural stones are grey to white and tend to be $> 2.0 \text{ g/cm}^3$; the masonries are brown to reddish and close to $< 2.0 \text{ g/cm}^3$. Concrete and natural stone are rich to exclusively made up of calcite, with high amounts of CaO ($> 40 \text{ wt.}\%$) and LOI (volatiles, $\text{CO}_2 + \text{H}_2\text{O}$). The masonries are instead calcite-, CaO- ($< 25 \text{ wt.}\%$) and LOI-poor ($< 8 \text{ wt.}\%$) but enriched in SiO_2 (45 to 70 wt.%), quartz and/or cristobalite, with significant amount of Al_2O_3 (12 to 20 wt%). S and Cl contents are similar among concrete, bricks and perforated bricks. Some CDW sample is susceptible to release relative high Cr content.

The petrography of these CDW concretes are similar among geographical areas with abundance of limestones used like aggregates. In limestone-poor areas CDW are SiO_2 - and Al_2O_3 -rich, reflecting the prevalence using of masonry and/or silicate-rich construction materials. Each geographical area can be characterised by peculiar CDW. In turn, the knowledge of mesoscopic, physical and petrographic aspects have to be known for planning adequate sorting methods, promoting upcycling reusing applications.

1. Introduction.

53 Construction and demolition waste (CDW) are all solid materials deriving from civil engineer-
54 ing works (buildings, roads, bridges, etc.), as well as from their demolition, restoration and/or collapse
55 due to natural or man-induced causes (e.g. earthquakes, landslides). CDW are extremely abundant in
56 both the EU and Italy, as summarised in [Figs. S1a, b](#). They are mainly composed of inert materials,
57 i.e. “ceramic-like” solids (concrete, mortars, cement, tiles, roof-tiles, bricks, natural stone, etc.), plus
58 asphalt, metals, plastics, textiles, wood, glass, RAEE (waste of electric and electronic equipment),
59 soils and/or dredging materials ([Figs. S1c, d](#)) (e.g. [Blengini & Garbarino, 2010](#); [Vitale et al., 2017](#)).
60 Commonly, inert ceramic-like CDW (hereafter only CDW) are collected separately from asphalt,
61 wood, plastics, metals, and textiles waste, and/or routinely separated from them ([Martín-Morales et](#)
62 [al., 2011](#); [Di Maria et al., 2013](#); [Ulsen et al., 2013](#); [Bonifazi et al., 2017a](#); [Neto et al., 2017](#); [Ambros](#)
63 [et al., 2019](#)) ([Fig. S1d](#)).

64 By contrast, the separation of heterogeneous CDW in relative homogeneous sub-populations is
65 complex and expensive. In turn, their physico-mechanical and petrographic (meaning as chemical,
66 mineralogical and textural attributes) features are frequently variable in time and space determining
67 poorly measurable and predictable behaviours ([de Brito et al., 2005](#); [Gonçalves & de Brito, 2010](#);
68 [Coelho & de Brito, 2013](#)). This heterogeneity strongly limits their reusing; frequently, new construc-
69 tion materials prepared with them may be characterized by low quality mechanical properties ([Coelho](#)
70 [& de Brito, 2013](#)). As a result, most CDW are low price materials, downcycling reused mainly for
71 road foundations, foundation slab, and cavity fillings ([Coelho & de Brito, 2013](#); [Di Maria et al., 2013](#)
72 [and 2016](#); [Gálvez-Martos et al., 2018](#)).

73 From a petrographic and materials science perspective, CDW are multi-phases solids made up
74 of silicate and/or carbonate minerals and glasses. The petrography of construction materials is still
75 poorly investigated and known: specifically, only a limited number of studies worldwide investigated
76 their mineralogical and/or chemical (i.e. petrographic) features ([Bianchini et al., 2005 and 2020](#);
77 [Limbachiya et al., 2007](#); [Rodrigues et al., 2013](#); [Alexandridou et al., 2014](#); [Komnitsas et al., 2015](#);
78 [Moreno-Perez et al., 2018](#); [Panizza et al., 2018](#); [Frias et al., 2020](#)). The petrography of CDW can be

79 variable as a function of available lithotypes (rocks), architectural and historical styles, as well as
80 national (past and present) regulations of a geographical area. Consequently, it is important to con-
81 strain the most salient petrographic features of construction materials and their derived waste for
82 several geographical areas worldwide.

83 In this paper, the most abundant and frequent ceramic-like CDW randomly sampled in the
84 Abruzzo region, Central Italy, were investigated. To the best of the authors' knowledge, they were
85 never investigated, although this region can be representative of several Italian (Apennines, Dolo-
86 mites) and Mediterranean (Greece, southern France, Albania) geographical and geological areas,
87 mainly characterised by limestone, sandstone and claystone lithotypes, including their incoherent to
88 poorly lithified dismantled and re-sedimented deposits ([Geological Map at 1:500 000 scale; Vola et](#)
89 [al., 2011](#)). Moreover, the Abruzzo region and its surroundings areas were repeatedly hit by earth-
90 quakes in the last decades, causing the loss of many human lives and accumulation of huge amounts
91 of CDW rubbles in the most damaged cities ([Galli et al., 2017](#)).

92 The aim of this study is to characterise common and representative single CDW samples from
93 the Abruzzo region via their mesoscopic, physical features and mineralogy (crystalline and non-crys-
94 talline attributes) by X-Ray Powder Diffraction (hereafter XRPD) analysis. Then, a sub-set of them
95 was also characterised with X-Ray Fluorescence Wavelength Dispersive Spectroscopy (hereafter
96 XRF-WDS) to quantify the chemical features. In addition, the potential release of chemical species
97 from this CDW was also assessed. Finally, the petrographic features of the CDW from Abruzzo have
98 been compared with those from other geographical and geological regions.

99

100 **2. Materials and methods**

101 **2.1 Mesoscopic and physical features.** The 18 single CDW samples considered here were col-
102 lected in various cities and towns of the Abruzzo region, according to their mesoscopic appearance
103 in the field. The most frequent and common construction of these waste materials were selected for
104 successive characterisations. . The CDW samples were classified in several groups according to their

mesoscopic appearance and commercial using: concrete (4), natural stone (Apennines carbonate) (2), bricks (3), tiles (3), roof tiles (3) and perforated bricks (3) (Table S1 and Fig. S2). In Fig. S2, the diameter of the mortar is about 5 cm.

The mesoscopic colours of the samples are qualitatively evaluated by eye on either bulk and as-received samples and their corresponding powders, obtained after grinding a portion of it for further analyses (see below). The texture refers to the classical petrographic observations and discrimination of grains in rocks used in Earth Sciences (Merico et al., 2020; Giuliani et al., 2020), such as: i) aphanitic and phaneritic for grains invisible ($<$ some tens of μm) and visible ($>$ some tens of μm) by the naked-eye or an optical lens (10 X), respectively. The porphyric texture refers to phaneritic grains immersed in an aphanitic matrix. The density was measured by weighing a relatively large piece (some cm^3) of each sample and measuring the volume with a water bath (graduated Becker).

2.2 XRPD (X-ray powder diffraction). The crystalline and non-crystalline phases were analysed via XRPD. For each bulk sample, about 10/20 g were grinded under alcohol using an electrical grinder: the produced powders had crystallite sizes of few hundreds of μm . About 2/3 g of each of these powders were dried and further grinded for 10 minutes again under alcohol, using an agate pestle and mortar. The final powdered samples were homogeneous and with crystallites sizes below 10 μm . Each fine powder was mounted into a cylindrical nominally zero-background Si sample holder, with a random distribution of crystallites. Using a zero-background Si sample holder allows qualitatively detecting the presence of non-crystalline phases.

Each powdered sample was analysed with a SIEMENS D-5000, with a Bragg-Brentano θ -2 θ configuration, equipped with $\text{CuK}\alpha$ radiation and a Ni filter. Each XRPD pattern was collected from 4 to 80° of 2 θ , with a step scan of 0.02° and counting time of 4 s per step. Each XRPD pattern was thus recorded in approximately 8 hours. The obtained XRPD patterns were first checked for the presence of non-crystalline content by observing some background shoulder (Walter et al., 2013; Boncio et al., 2020). Then, the Bragg reflections were assigned by search-match comparisons to crystalline standards contained in the inorganic crystal structure database (ICSD) (Boncio et al., 2020). The

131 search-match identification of measured Bragg reflections started from the most intense peaks; the
132 XRPD standards that better reproduce either the 2 θ positions or the relative intensities of measured
133 Bragg reflections were used to identify the minerals in each sample (Fig. 1).

134 The abundance of crystalline phases (wt%), was semi-quantitatively evaluated using the RIR
135 (reference intensity ratio) method (Hubbard and Snyder, 1998; Johnson and Zhou, 2000; Chipera and
136 Bish, 2013; Boncio et al., 2020). The RIR method used here is implemented in the software package
137 “Match! version 3.9.0” (Crystal Impact, 2019). The RIR compares the intensity scaling factor of each
138 mineralogical phase (I) with a “virtual” corundum crystalline phase (I_{cor.}), which is not necessarily
139 present in the XRPD patterns. The ratio “I/I_{cor.}” is then used for assessing semi-quantitatively the
140 content (wt%) of each crystalline phase (Table S2).

141 **2.3 XRF-WDS.** Based on the XRPD outcomes, the chemical compositions of 11 samples (MPA-
142 10, MPA-18, MPA-04, MPA-14, MPA-07, MPA-11, MPA-09, MPA-16, MPA-01, MPA-05 and
143 MPA-15) were obtained using a XRF-WDS analysis (Table S3 and S4). The major, minor and trace
144 elemental features were obtained both using a Philips PW 1480 spectrometer, calibrated using exter-
145 nal standards by Chunshu et al. (1996) following the procedure defined by Gazzulla Barreda et al.
146 (2016), and an ARL Advant-XP spectrometer, following the full matrix correction method proposed
147 by Lachance and Traill (1966). The accuracy is < 5% for major oxides, and < 10% for trace element.
148 Volatiles were determined by loss on ignition (LOI) at 1000 °C.

149 *Leaching test.* Leaching tests were also performed (Table S5). The adopted leaching protocol
150 was modified from the UNI EN 12457-Part 2 (2004) and also reported in Bianchini et al. 2020.
151 Briefly, 1 g of CDW powder was soaked with 10 ml of deionised water for 24 h and the obtained
152 solution was centrifuged at 3000 rpm for 10 min and filtered at 45 μ m (Minisart®NML syringe cel-
153 lulose acetate filters). The composition of leachates (expressed in mg/l) was obtained by inductively
154 coupled plasma mass spectrometry (ICP-MS) using a Thermo X-series spectrometer instrument on
155 samples previously diluted 1:5 by deionised Milli-Q water (resistivity of ca. 18.2 M Ω x cm). Instru-
156 mental calibration was carried out using certified solutions and a known amount of Re and Rh was

also introduced in each sample as an internal standard. Accuracy and precision were determined using several international reference standards, being lower than 10% of the measured value, with detection limits in the order of 0.001 mg/l.

3. Results

3.1 Mesoscopic texture. The mesoscopic appearance and texture, as well as density of the four concrete, two natural stone, three brick, three tile, three roof tile and three perforated brick CDW samples are reported in Table S1 and displayed in Fig. S2. The colour of bulk as-received concrete is invariably pale grey and that of natural stone is either grey or white. All the other materials, i.e. tiles, roof tiles, bricks and perforated-bricks, except the sample MPA-07, are coloured (Table S1 and Fig. S2).

The MPA-03, MPA-10, MPA-13 and MPA-18 concrete samples are all characterized by a porphyric texture, with large and visible clasts (aggregate) immersed in an aphanitic matrix made of cementitious binders. The natural stones are either aphanitic (MPA-08) or porphyric (MPA-19) (Table 2). The bricks MPA-02 and MPA-04 are porphyric and the MPA-14 aphanitic, the MPA-07, MPA-11 and MPA-17 tiles are invariably aphanitic, while the roof tiles MPA-09 and MPA-12 are aphanitic and only the MPA-16 is porphyric (Table S1). Finally, the two perforated bricks MPA-01 and MPA-05 are aphanitic and the MPA-14 is instead porphyric.

3.2 Density. The density of concrete varies between 2.02 and 2.49 g/cm³, and that of natural stone between 2.1 and 2.74 g/cm³. The density of the four bricks ranges from 1.7 to 2.25 g/cm³, that of the three tiles from 1.83 to 2.3 g/cm³, that of roof tiles from 1.71 to 2.22 g/cm³ and that of the three perforated bricks is invariably < 2 g/cm³, i.e. between 1.73 and 1.94 g/cm³ (Table S1).

3.3 Crystalline (and non-crystalline) phases. The XRPD spectra are stacked in Fig. 1, as a function of groups (Table S2). A more detailed visualization of them per group is reported in Figs. S3a, b, c, d, e, f, while a comparison of the crystalline phases' content is provided in Fig. 2. All concrete samples show significant amounts of calcite and quartz and the MPA-13 and MPA-18 spectra also display illite and plagioclase. Overall, the mineralogical composition of these four concrete

183 samples is similar, while the presence of non-crystalline phase is undetected or barely appreciable
184 (Figs. 1 and S3a). The four concrete samples are composed of calcite with a range comprised between
185 56 and 88 wt.%, plus a moderate to significant amount of quartz ranging from 8 to 27 wt.%; plagioclase
186 feldspars and illite sheet-silicates are absent or with moderate to minor contents, i.e. up to 19
187 and 5 wt.%, respectively (Table S2 and Fig. 2). The two stone samples are made up exclusively of
188 calcite and free of non-crystalline materials (Figs. 1 and S3b).

189 The other four groups are notably different from concrete, since they are characterised by silicate
190 crystalline phases and free of calcite, except for the roof tiles MPA-12 and MPA-16 (Table S2
191 and Figs. S3a, b, c, d, e, f). Quartz and cristobalite, the two SiO₂ polymorphs of SiO₂, are the most
192 abundant crystalline phases (Table S2 and Figs. 1, S3a, b, c, d, e, f). Indeed, the non-crystalline phases
193 cannot be characterised by XRPD, but should be also SiO₂-rich according to the broad shoulder position,
194 the prevalent chemical system and its determination for a sub-set of samples (see below).

195 The bricks contain quartz, cristobalite, clinopyroxene, alkali-feldspar, plagioclase, melilite and
196 mullite. The MPA-04 and MPA-14 samples display a given amount of non-crystalline phases, the
197 MPA-02 and MPA-04 samples are relative similar, whereas MPA-14 is by far the most different
198 sample from the previous two (Table S2, Figs. 1, S3c and 2).

199 The three perforated bricks are composed of quartz, clinopyroxene, plagioclase, biotite and melilite,
200 and free of calcite (Figs. 1 and S3f). Their mineralogical content is relatively similar for clinopyroxene
201 and plagioclase, ranging respectively between 12 to 26 and 7 to 14 wt.%; melilite is instead
202 either absent or up to 24 wt.%, while quartz changes from 45 to 75 wt.% (Table S2 and Fig. 2).

203 The three tiles are mainly composed of quartz and cristobalite, plus minor plagioclase and variable
204 amount of non-crystalline phases, showing very similar XRPD patterns, mirroring a very close
205 crystalline and non-crystalline content of phases (Figs. 1 and S3d). In line, they are made of 70 to 100
206 wt.% of quartz, an amount of cristobalite and plagioclase switching between 6 to 8 and 24 to 11 wt.%,
207 plus non crystalline phase in sample MPA-07 (Table S2 and Fig. 2).

208 The three roof tiles contain quartz and cristobalite, calcite, clinopyroxene, plagioclase, biotite
209 and melilite, whilst non-crystalline phases were undetected (Figs. 1 and S3e). Overall, MPA-12 and
210 16 show the wt.% of very similar crystalline phases. Differently, MPA-09 has no calcite and major
211 values of clinopyroxene and plagioclase, relative to MPA-12 and 16 (Table S2 and Fig. 2).

212 Concrete is rich to very rich in cc, ornamental stones are made of cc only, whereas bricks, tiles,
213 roof tiles and perforated bricks are cc-poor and -free, but rich in silicate crystalline phases. The other
214 data from previous studies are from the following geographical regions: 1* - southern Greece (Alex-
215 andridou et al., 2014), central Spain (Frias et al., 2020), Portugal (Rodrigues et al., 2013) and Veneto
216 region of Italy (Panizza et al., 2018). The acronyms are n.s.: natural stone, cc: calcite, do: dolomite,
217 qz: quartz, cri: cristobalite, pl: plagioclase, kf: k-feldspar, cpx: clinopyroxene, il: illite, bi: biotite, me:
218 melilite, mu: mullite, kao: kaolinite, gy: gypsum, port: portlandite, thau: thaumasite, ettr: ettringite,
219 hema: hematite and ncp: non-crystalline phase.

220 **3.4 Bulk chemical composition.** The major chemical species are expressed in oxide weight per
221 cent (wt. %), while the minor and trace elemental features are reported in mg/kg (Tables S3 and S4).
222 Since the two stone samples (Apennines limestone) are composed of calcite only (Fig. 1 and S3b),
223 their chemical compositions are very close to CaCO_3 and were thus not analysed. The bulk major
224 oxide compositions of the 11 selected samples are compared in Figs. 6 and 7.

225 The first important difference is the significant distinction between concrete and all the other
226 groups. The former is very rich in CaO (> 40 wt.%) plus LOI (> 25 wt.%), with moderate amounts of
227 SiO_2 (< 27 wt.%), poor in Al_2O_3 (< 2.5 wt.%) and with very low contents of Fe_2O_3 (< 1.5 wt.%), MgO
228 (< 1 wt.%) and alkalis (< 0.6 wt.%) (Table S3 and Figs. 3, 4). The high content of LOI is related to the
229 CO_2 content derived from calcite, as measured by XRPD (Table S2 and Fig. 2). Conversely, brick, tile,
230 roof tile and perforated brick groups are invariably rich in SiO_2 (> 47 and < 71 wt.%) and Al_2O_3 (> 12
231 and < 20 wt.%), while relatively poor in CaO (< 24 wt. %): tiles are extremely poor in CaO (< 3 wt.%)
232 (Table S3 and Figs. 3, 4). The other oxides are relatively abundant: notably, Fe_2O_3 is around 1.5 wt.%
233 for tiles but approximately 5 wt.% for bricks, roof tiles and perforated bricks (Table S3 and Figs. 3, 4).

234 A similar situation is shown by MgO and alkalis (Figs. 3, 4). The tiles are richer in Al_2O_3 and poorer in
235 Fe_2O_3 and MgO compared to bricks, roof tiles and perforated bricks (Table S3 and Figs. 3, 4). Notably,
236 the amounts of CaO and respective LOI of these groups show an opposite correlation, testifying that
237 their LOI are poorly related to the content of calcite (Fig. 4).

238 Overall, all the minor and trace element contents are lower than 1 wt.% (Fig. 5). The differences
239 and similarities observed for major oxide bulk chemical compositions in and between CDW groups
240 are not mirrored by the content of minor and trace elements (Tables S3 and S4 and Figs. 5, 6). For
241 example, concrete shows a remarkable similarity with bricks and perforated bricks, especially for
242 MPA-10, MPA-18, MPA-14 and MPA-05; the brick MPA-04 and the two perforated bricks MPA-01
243 and MPA-05 samples are very close in minor and trace element contents (Figs. 5, 6). By contrast, the
244 two tiles MPA-07 and MPA-11 are similar to MPA-09 and to a lesser extent with the MPA-16 roof
245 tiles (Figs. 5, 6).

246 The content of critical S and Cl are relatively high for both concrete samples (MPA-10 and
247 MPA-18) and the brick MPA-14 and the perforated brick MPA-05 samples; the tiles and roof tiles
248 are instead poor in S and Cl (Table S4 and Figs. 5, 6). Remarkably, the amount of Pb is extremely
249 low for all samples except the MPA-11 tile that is exceptionally rich in Pb (Table S4 and Figs. 5, 6).
250 Finally, the amount of Sc, V, Cr, Co, Ni, Cu, Zn and As metals is several hundreds of mg/kg; concrete
251 contains the lowest contents (Table S4 and Figs. 5, 6).

252 **3.5 Leachates.** The possible release of dangerous chemical species by CDW is an important
253 issue in terms of toxicological and environmental issues (Bianchini et al., 2020). The most significant
254 and potentially harmful elements and their threshold values (according to the Italian norms) are re-
255 ported in Table S5 as a function of the CDW groups; the most valuable metallic elements are also
256 plotted in Fig. 7. The release of any element is invariably and by far lesser than 1 mg/l. According to
257 the Italian legislation, only As and Cr in some samples are higher than the corresponding limits. In
258 fact, both bricks, the MPA-07 tile and the MPA-15 perforated brick samples, have As contents higher

259 than 0.01 mg/l; in parallel, the Cr content of the two concrete and the MPA-05 perforated bricks
260 samples have significant higher amounts than the admissible 0.05 mg/l value (Table S5 and Fig. 7).

261

262 4. Discussion

263 The petrographic heterogeneity of CDW is the main limitation for their upcycling reuse. For
264 instance, RAC (recycled aggregate concrete) prepared with masonry materials (MRA: masonry recy-
265 cled aggregates) and/or the attached fraction of cement binders in RCA (recycled concrete aggregates)
266 tend to have poorer performance than conventional concrete (e.g. de Brito et al., 2005; Evangelista et
267 al., 2007; Gonçalves & de Brito, 2010; Agrela et al., 2011; Coelho & de Brito, 2013; Bravo et al.,
268 2015; Bravo et al., 2020). In parallel, the quantification of the mesoscopic, physical and petrographic
269 differences is critical for the possible elimination of a heterogeneous CDW, like that occurring under
270 uncontrolled demolitions, illegal disposal and rubble from earthquakes (Martín-Morales et al., 2011;
271 Di Maria et al., 2013; Ulsen et al., 2013; Bonifazi et al., 2017a; Neto et al., 2017; Ambros et al.,
272 2019).

273 The determination of the mesoscopic, physical, mineralogical and chemical attributes of single
274 CDW samples from Abruzzo performed here unveils several aspects. The colour (appearance), tex-
275 ture, density, mineralogy and chemical composition show high to moderate similarities within each
276 group (concrete, ornamental stone, brick, tile, roof tile and perforated bricks) (Figs. 2, 3, 4, S2). By
277 contrast, the differences are clearer between different groups, especially between concrete and natural
278 stone and the other four groups (Figs. 2, 3, 4, S2).

279 Typical concrete, mortars and stone from Abruzzo are white to grey, whereas all the other ma-
280 sonry CDW are coloured, except the MPA-07 grey tile (Table S1 and Fig. S2). Similarly, concrete
281 and stone have moderate to high density (2 to 2.7 g/cm³), whereas the perforated bricks' density is
282 always and markedly lower than 2 g/cm³. The other groups are instead more scattered, with a ten-
283 dency to be less than 2 g/cm³ (Table S1); specifically, the MPA-04 (brick), MPA-17 (tile) and MPA-
284 12 (roof tile) samples overlap the average density of concrete (2.2 ± 0.2 g/cm³) (Table S1). All these

mesoscopic features suggest that the separation of CDW from Abruzzo, as well as those from similar geographical and geological regions, can only be poorly enforced using processing based on density (e.g. [Coelho & de Brito, 2013](#); [Di Maria et al., 2013 and 2016](#); [Ambros et al., 2017](#); [Bonifazi et al., 2017a](#); [Hu et al., 2019](#)) but more efficiently with procedures based on colour ([Gokyyu et al., 2011](#)). Hence, an initial heterogeneous CDW from Abruzzo can be separated relatively well in two fractions using density and, especially, colour attributes: the first, enriched in concrete and stone, the second in masonry-rich CDW materials.

These mesoscopic (mainly colour) and physical differences between concrete and stone and masonry materials reflect petrographic attributes. The former are rich (> 50 wt.%) to exclusively (100 wt.%) made up of calcite and obviously present high values (> 50 wt.%) of CaO and LOI (volatile components), reflecting the high amount of CO₂ of the carbonate aggregates ([Figs. 1, 2, 3](#)). On the other hand, bricks, perforated bricks, tiles and roof tiles are calcite-poor or -free and rich in crystalline and non-crystalline silicate phases ([Figs. 1, 2, 3](#)). Thereby, the separation of concrete from masonry CDW materials in Abruzzo can be further enhanced by a separation based on chemical compositions ([Serranti et al., 2015](#); [Bonifazi et al., 2017b, 2018, 2019](#)), since the former are CaO-rich and SiO₂-poor, while the latter show the inverse characteristics.

The amounts of the various crystalline phases in the CDW from Abruzzo are compared with those provided in four previous studies performed on CDW from the Veneto region in north-east of Italy ([Panizza et al., 2018](#)), central Spain ([Frias et al., 2020](#)), Portugal ([Rodrigues et al., 2013](#)) and southern part of Greece ([Alexandridou et al., 2014](#)). These investigations deal with either mixed CDW or selected groups like in here ([Table S2](#)). Overall, the typical crystalline phases solidified from the cement bindings fraction of concrete, i.e. ettringite, thaumasite, portlandite, etc., are undetected or detected with very low amounts ([Table S2](#) and [Fig. 2](#)). The mineralogy of CDW concrete from Abruzzo is very similar to that analysed in southern Greece ([Alexandridou et al., 2014](#)) and relatively close to that coming from Veneto ([Panizza et al., 2018](#)). By contrast, the mixed CDW from Spain ([Frias et al., 2020](#)) and Portugal ([Rodrigues et al., 2013](#)) show a low to moderate amount of carbonates (calcite + dolomite) ([Table S2](#) and

311 Fig. 2), probably reflecting the mixing of concrete with masonry materials, as well as different litholog-
312 ical features. Indeed, the Abruzzo, Veneto and southern Greece regions are extremely rich in carbonate
313 rocks that were used to build most human structures.

314 Due to their crystalline and non-crystalline phases, concrete (and natural stone) and masonry CDW
315 from Abruzzo are significantly different (Figs. 3, 4). Again, the former is enriched in CaO and LOI (CO₂)
316 and poor in SiO₂, Al₂O₃ and alkalis (Table S3 and Fig. 4). A more robust reappraisal of the similarities
317 and differences between CDW from different regions worldwide can be obtained through their chemical
318 features. In Table S3, the most significant studies, for which quantitative chemical characterisation of
319 CDW was provided, were reported. These data are compared in triangular diagrams in Fig. 8.

320 The concrete groups from Abruzzo and southern Greece (Alexandridou et al., 2014) are both very
321 rich in CaO and poor in SiO₂ + Al₂O₃, in line with XRPD outcomes (Fig. 2); conversely, the three CDW
322 concrete samples (RCA1, RCA2 and RCA3 in Table S3) from London (UK) (Limbachiya et al., 2007)
323 are poor in CaO and rich in SiO₂. The former two groups again reflect the extremely high abundance
324 of carbonate rocks in Central Italy and southern Greece, whereas those of Limbachiya et al. (2007)
325 mirror the paucity of carbonate rocks around London. At the same time, all the CDW from other re-
326 gions, made up of mixed CDW, have a content of CaO invariably lower than that of SiO₂ + Al₂O₃, SiO₂
327 + MgO + Fe₂O₃ and SiO₂ + Na₂O + K₂O (Fig. 8). These features reflect both their mixed CDW signature
328 and the scarcity of carbonate rocks from these areas. It is finally relevant to highlight that CDW from
329 Abruzzo is strongly different from that sampled in Ferrara, Emilia-Romagna region. These two areas
330 are located at a distance of only few hundreds of km, have been inhabited for thousands years and their
331 architectural histories are close. Nevertheless, their construction materials are significantly different,
332 due to the abundance of carbonates rocks in Abruzzo and their scarcity in the Po River plain settlements
333 (Vola et al., 2011). These outcomes evidence the necessity to characterise the petrography of CDW
334 at a local level to identify their main chemical and mineralogical features. These aspects could be
335 useful to design sorting procedures based also on petrography.

336

5. Conclusion

As a general conclusion, areas rich in carbonate rocks, i.e. limestone, can be expected to share similar features of their CDW concrete such as: a relative high density, a whitish to pale grey colours, high amounts of calcite/dolomite crystalline phases, as well as being CaO- and CO₂-rich (Figs. 3, 8, S2). These aspects make CDW from Abruzzo and similar regions able to be sorted and separated in two main and relatively homogeneous concrete and masonry groups, *via* macroscopic colour investigation and whole chemical sorting procedures. Finally, the leaching test shows that some samples exceed the Italian Threshold Values of Heavy Metals (TVHM) limit (Italian Legislative Decree 152, 03/04/2006) for Cr and As (Table S5 and Fig. 7). These aspects are already reported for other CDW (Frias et al., 2002; Eštoková et al., 2012) and further highlight the necessity to characterise routinely the petrography and geochemistry, as well as the leachates, of CDW worldwide.

Acknowledgements. The authors are grateful to Prof. Pinjing H.E. for the editorial work and the two anonymous reviewers that improved the quality of this study. This research has been conducted during the PhD project of Galderisi A. supported with funds from the Italian PON program promoting the industrial PhD awarded to G. Iezzi and by the “Fondi Ateneo of the University G. D’Annunzio”.

References

- Agrela F., Sánchez de Juan M., Ayuso J., Geraldés V.L, Jiménez J.R., 2011. Limiting properties in the characterisation of mixed recycled aggregates for use in the manufacture of concrete. *Construction and Building Materials*, 25, 10, pp. 3950-3955.
- Alexandridou C., Angelopoulos G. N., Coutelieris F. A., 2014. Physical, Chemical and mineralogical characterization of construction and demolition waste produced in Greece. *International Scholarly and Scientific Research & Innovation*, 8(9).

362 Ambros W.M., Sampaio C.H., Cazaciu B.G., Miltzarek G.L., Miranda L.R., 2017. Usage of air
 363 jigging for multi-component separation of construction and demolition waste. *Waste Management*,
 364 60, pp. 75–83

365 Ambrós W.M., Sampaio C.H., Cazaciu B.G., Conceição P.N., dos Reis G.S., 2019. Some ob-
 366 servations on the influence of particle size and size distribution on stratification in pneumatic jigs.
 367 *Powder Technology*, 342, pp. 594–606.

368 Blengini G. A., Garbarino E., 2010. Resources and waste management in Turin (Italy): the role
 369 of recycled aggregates in the sustainable supply mix. *Journal of Cleaner Production*, 18, pp. 1021–
 370 1030.

371 Bianchini G., Martucci A., Vaccaro C., 2002. Petro-archaeometric characterisation of "cotto
 372 ferrarese": bricks and terracotta elements from historic buildings of Ferrara. *Per. Mineral.*, 71, special
 373 issue: *Archaeometry and Cultural Heritage*, 101-111.

374 Bianchini G., Marrocchino E., Tassinari R., Vaccaro C., 2005. Recycling of construction and dem-
 375 olition waste materials: a chemical–mineralogical appraisal. *Waste Management*, 25, pp. 149–159.

376 Bianchini G., Ristovski I., Milcov I., Zupac A., Natali C., Salani G. M., Marchina C., Brombin
 377 V., Ferraboschi A., 2020. Chemical Characterisation of Construction and Demolition Waste in Skopje
 378 City and Its Surroundings (Republic of Macedonia). *Sustainability* 12, 2055.

379 Boncio P., Amoroso S., Galadini F., Galderisi A., Iezzi G., Liberia F., 2020. Earthquake-in-
 380 duced liquefaction features in a late Quaternary fine-grained lacustrine succession (Fucino Lake, It-
 381 aly): Implications for microzonation studies. *Engineering Geology*, 272, 105621.

382 Bonifazi G., Serranti S., Potenza F., Luciani V., Di Mario F., 2017a. Gravity packaging final
 383 waste recovery based on gravity separation and chemical imaging control. *Waste Management*, 60,
 384 pp. 50–55.

385 Bonifazi G., Palmieri R., Serranti S., 2017b. Concrete drill core characterization finalized to
 386 optimal dismantling and aggregates recovery. *Waste Management*, 60, pp 301–310.

387 Bonifazi G., Palmieri R., Serranti S., 2018. Evaluation of attached mortar on recycled concrete
 388 aggregates by hyperspectral imaging. *Construction and Building Materials*, 169, pp 835–842.

389 Bonifazi G., Capobianco G., Palmieri R., Serranti S., 2019. Hyperspectral imaging applied to
 390 the waste recycling sector. *Spectroscopy Europe*, 31, 2, pp 8-11.

391 Bravo M., de Brito J., Pontes J., Evangelista L., 2015. Mechanical performance of concrete
 392 made with aggregates from construction and demolition waste recycling plants. *Journal of Cleaner*
 393 *Production*, 99, pp. 59–74.

394 Bravo M., Duarte A. P. C., de Brito J., Evangelista L., Pedro D., 2020. On the development of
 395 a technical specification for the use of fine recycled aggregates from construction and demolition
 396 waste in concrete production. *Materials*, 13, 4228.

397 Cachim P.B., 2009. Mechanical properties of brick aggregate concrete. *Construction and Build-*
 398 *ing Materials*, 23, pp. 1292–1297.

399 Chipera S.J. and Bish D.L., 2013. Fitting full X-Ray diffraction patterns for quantitative analy-
 400 sis: a method for readily quantifying crystalline and disordered phases. *Advances in Materials Physics*
 401 *and Chemistry*, 3, 47–53.

402 Chunshu, W., Mingcai, Y., Wenhua, Z., Qinghua, C., Tiexin, G., 1996. Chinese synthetic silicate
 403 and limestone certified reference materials for spectral analysis. *Geostandard Newsletter*. 20, 57–64.

404 Coelho A., de Brito J., 2013. Economic viability analysis of a construction and demolition waste
 405 recycling plant in Portugal e part I: location, materials, technology and economic analysis. *Journal of*
 406 *Cleaner Production*, 39, pp. 338-352.

407 Di Maria F., Micale C., Sordi A., Cirulli G., Marionni M., 2013. Urban mining: Quality and
 408 quantity of recyclable and recoverable material mechanically and physically extractable from residual
 409 waste. *Waste Management*, 33, pp. 2594–2599.

410 Di Maria F., Bianconi F., Micale C., Baglioni S., Marionni M., 2016. Quality assessment for
 411 recycling aggregates from construction and demolition waste: An image-based approach for particle
 412 size estimation. *Waste Management*, 48, pp. 344–352.

413 Ente Nazionale Italiano di Unificazione. UNI EN 12457—Part 2 (2004)—Characterisation of
414 waste-leaching-compliance test for leaching of granular waste materials and sludges—Part 2: One
415 stage batch test at a liquid to solid ratio of 10 l/kg for materials with particle size below 4 mm (without
416 or with size reduction); Ente Nazionale Italiano di Unificazione: Milan, Italy, 2004.

417 Eštoková A., Palaščáková L., Singovszkáb E., Holubb M., 2012. Analysis of the chromium
418 concentrations in cement materials. *Procedia Engineering*, 42, pp. 123-130.

419 European Parliament. Directive 2008/98/CE of the European Parliament and of the Council of
420 19 November 2008 on Waste and Repealing Certain Directives. O. J. Eur. Union 2008, L312, 3–30.
421 <https://eur-lex.europa.eu/legal-content/EN/TXT/?uri=celex%3A32008L0098>

422 Eurostat, 2017. Generation of Waste by Waste Category, Hazardousness and NACE Rev 2 Ac-
423 tivity. https://appsso.eurostat.ec.europa.eu/nui/show.do?dataset=env_wasgen&lang=en

424 Evangelista L., de Brito J., 2007. Mechanical behaviour of concrete made with fine recycled
425 concrete aggregates. *Cement and Concrete Research*, 29, 397–401.

426 Favaretto P., Hidalgo G.E.N., Sampaio C.H., de Almeida Silva R., Lermen R.T., 2017. Charac-
427 terization and use of construction and demolition waste from south of brazil in the production of
428 foamed concrete blocks. *Applied Science*, 7, 1090.

429 Frias M., Sánchez de Rojas MI, 2002. Total and soluble chromium, nickel and cobalt content in
430 the main materials used in the manufacturing of Spain commercial cements. *Cement and Concrete*
431 Composites, 32, pp. 435- 440.

432 Frias M., de la Villa R.V., Ramírez S.M., Carrasco L.F., Cociña E.V., Giménez R.G., 2020.
433 Multi-technique characterization of a fine fraction of CDW and assessment of reactivity in a
434 CDW/lime system. *Minerals*, 10, 590.

435 Gálvez-Martos J., Stylesb D., Schoenbergerd H., Zeschmar-Lahle B., 2018. Construction and
436 demolition waste best management practice in Europe. *Resources, Conservation & Recycling* 136,
437 166–178.

438 Galli, P., Castenetto, S., Peronace, E., 2017. The macroseismic intensity distribution of the 30
 439 October 2016 earthquake in Central Italy (Mw 6.6): Seismotectonic implications. *Tectonics* 36, 1–13.

440 Gazzulla Barreda, M.F., Rodrigo Edo, M., Orduña Cordero, M., Ventura Vaquer, M.J., 2016.
 441 Determination of minor and trace elements in geological materials used as raw ceramic materials.
 442 *Boletín de la Sociedad Española de cerámica y vidrio* 55, 185–196.

443 Giuliani L., Iezzi G., Vetere F.P., Behrens H., Mollo S., Cauti F., Ventura G., Scarlato P. (2020).
 444 Evolution of textures, crystal size distributions and growth rates of plagioclase, clinopyroxene, and
 445 spinel crystallized at variable cooling rates from a mid-ocean ridge basaltic melt. *Earth Science Re-*
 446 *views*, 204, 103165.

447 Gonçalves P., de Brito J., 2010. Recycled aggregate concrete (RAC) - Comparative analysis of
 448 existing specifications. *Magazine of Concrete Research*, 62(5), pp. 339–46.

449 Gokyyu, T., Nakamura, S., Ueno, T., Nakamura, M., Inoue, D., Yanagihara, Y., 2011. Sorting
 450 system for recycling of construction byproducts with Bayes' theorem-based robot vision. *Journal of*
 451 *Robotics and Mechatronics*, 23 (6), pp. 1066–1072.

452 Hu K., Chen Y., Naz F., Zeng C., Cao S., 2019. Separation studies of concrete and brick from
 453 construction and demolition waste. *Waste Management*, 85, pp. 396–404.

454 Hubbard C.R. and Snyder R.L., 1998. RIR - Measurement and use in quantitative XRD. *Powder*
 455 *Diffraction*, 3 (2), p. 74–77.

456 Komnitsas K., Zaharaki D., Vlachou A., Bartzas G., Galetakis M., 2015. Effect of synthesis
 457 parameters on the quality of construction and demolition wastes (CDW) geopolymers. *Advanced*
 458 *Powder Technology*, 26, pp. 368–376.

459 Johnson Q. and Zhou R.S., 2000. Checking and estimating RIR values. *Advances in X-ray*
 460 *Analysis*, 42, pp. 287–296.

461 Lachance G.R., Traill R.J., 1966. Practical solution to the matrix problem in X-ray analysis.
 462 *Canadian Journal of Spectroscopy*, 11, pp. 43–48.

463 Merico A., Iezzi G., Pace B., Ferranti L., Cremona M., Scafa M., Cavallo A., Colella A., Nazzari
 464 m., Scarlato P. (2020). Grain size and grain size distribution of a lithified fault core in carbonates
 465 rocks using multi-scale image analysis: The example of the San Benedetto-Gioia dei Marsi fault
 466 (Central Italy). *Journal of Structural Geology*, 134, 104017.

467 Morales M., Zamorano M., Moyano, A.R., Espinosa I.V., 2011. Characterization of recycled
 468 aggregates construction and demolition waste for concrete production following the Spanish struc-
 469 tural concrete code ehe-08. *Construction and Building Materials*, 25 (2), pp. 742–748.

470 Moreno-Pérez E., Hernández-Ávila J., Rangel-Martínez Y., Cerecedo-Sáenz E., Arenas-Flores A.,
 471 Reyes-Valderrama M. I., Salinas-Rodríguez E., 2018. Chemical and mineralogical characterization of
 472 recycled aggregates from construction and demolition waste from Mexico City. *Minerals*, 8, 237.

473 Neto R.O., Gastineau P., Cazacliu B.G., Le Guen L., Paranhos R.S., Petter C.O., 2017. An eco-
 474 nomic analysis of the processing technologies in CDW recycling platforms. *Waste Management*, 60,
 475 pp. 277–289.

476 Panizza M., Natali M., Garbin E., Tamburini S., Secco M., 2018. Assessment of geopolymers
 477 with Construction and Demolition Waste (CDW) aggregates as a building material. *Construction and*
 478 *Building Materials*, 181, pp. 119–133.

479 Rodrigues F., Carvalho M. T., Evangelista L., de Brito J., 2013. Physical-chemical and miner-
 480 alogical characterization of fine aggregates from construction and demolition waste recycling plants.
 481 *Journal of Cleaner Production*, 52, pp. 438-445.

482 Rukijkanpanich J., Thongchai N., 2019. Burned brick production from residues of quarrying
 483 process in Thailand. *Journal of Building Engineering*, 25, 100811.

484 Sabai S. M. M., Lichtenberg J. J., Egmond E. L., Florea M. V. M., Brouwers H.J.H., 2016.
 485 Construction and Demolition Waste Characteristics in Tanzania. *Journal of the Open University of*
 486 *Tanzania*, 23(1), pp 1-19.

487 Serranti S., Palmieri R., Bonifazi G., 2015. Hyperspectral imaging applied to demolition waste re-
 488 cycling: innovative approach for product quality control. *Journal of Electronic Imaging*, 24, 043003.

489 The Government of Italy. Legislative Decree 152/06 (2006) Norme in materia ambientale; Of-
490 ficial Gazette n. 88; The Government of Italy: Rome, Italy, 2006. (In Italian)

491 Ulsen C., Kahn H., Hawlitschek G., Masini E. A., Angulo S. C., 2013. Separability studies of
492 construction and demolition waste recycled sand. *Waste Management*, 33, pp. 656–662.

493 Vitale P., Arena N., Di Gregorio F., Arena U., 2017. Life cycle assessment of the end-of-life
494 phase of a residential building. *Waste Management*, 60, pp. 311–321.

495 Vola G., Berrab M., Rondenab E. (2011). Petrographic quantitative analysis of ASR susceptible
496 Italian aggregates for concrete. 13th Euroseminar on Microscopy Applied to Building Materials 14-
497 18 June 2011, Ljubljana, Slovenia.

498 Walter J.M., Iezzi G., Albertini G., Gunter M.E., Piochi M., Ventura G., Jansen E., Fiori F. (2013).
499 Enhanced crystal fabric analysis of a lava flow sample by neutron texture diffraction: a case study from
500 the Castello d’Ischia dome. *Geochemistry, Geophysics, Geosystems*, 14(1), pp. 179-196.

501

502

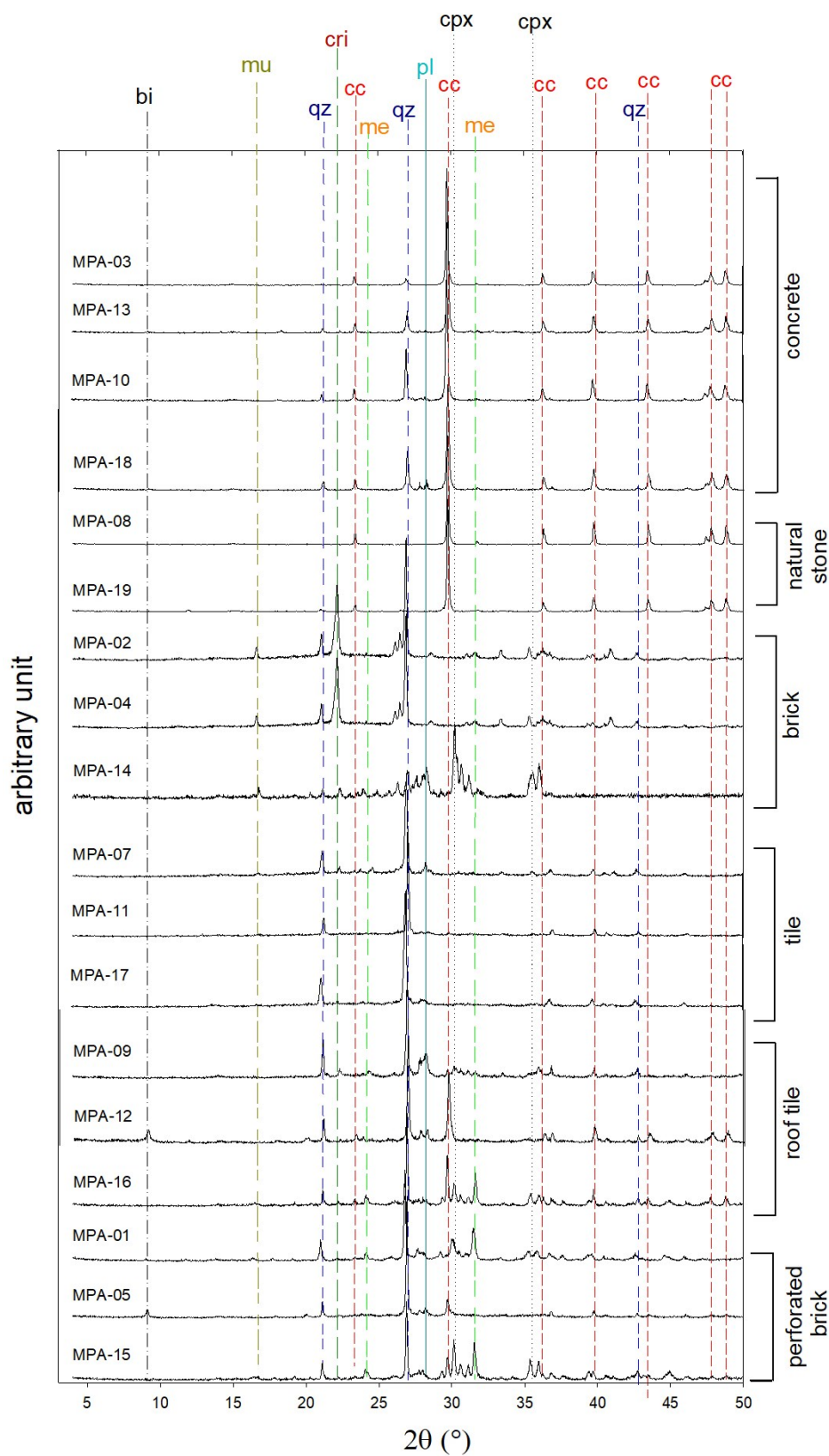


Fig. 1. Stacked XRPD patterns with indentified Bragg reflections to their corresponding crystalline standards from the ICSD database. A more detailed visualisation of these XRPD patterns is reported in Figs. S3a, b, c, d, e and f.

507
508
509
510
511
512
513
514
515
516
517
518
519
520
521
522
523
524
525
526
527
528
529
530
531
532

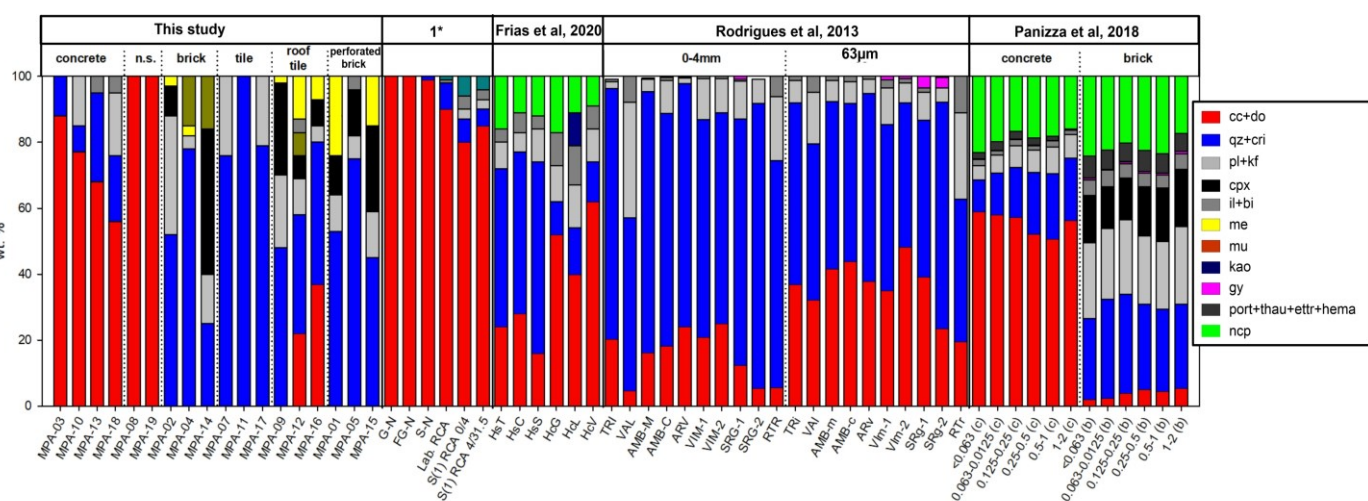


Fig. 2. Semi-quantitative content of crystalline phases (wt. %) by XRPD in the Abruzzo samples (this study, [Table S2](#)).

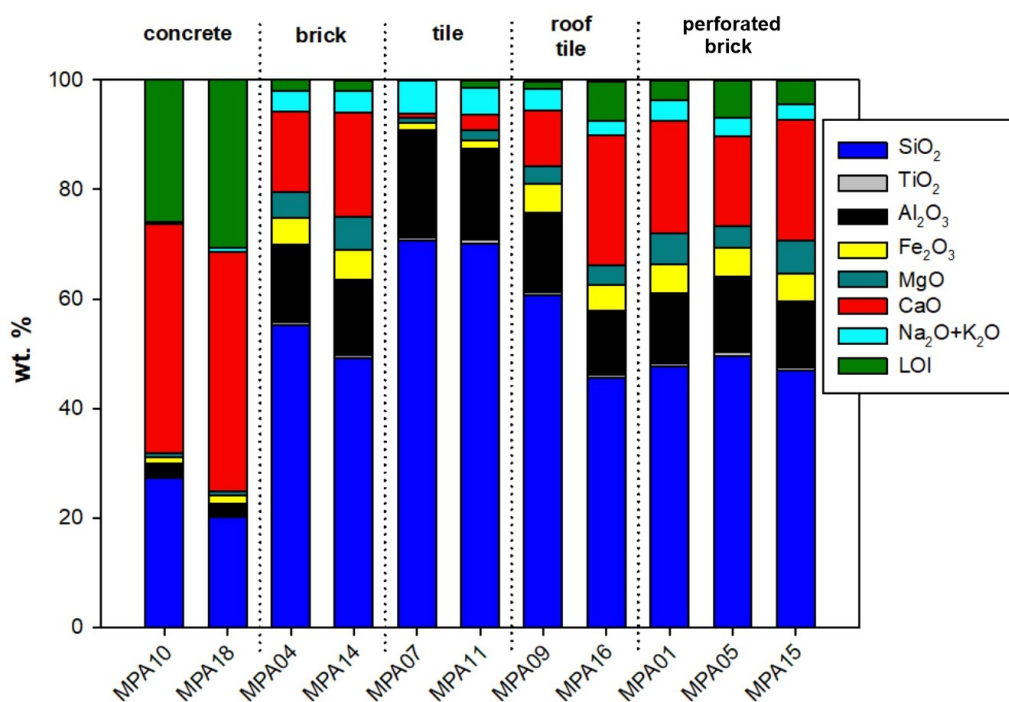


Fig. 3. Quantitative abundance of major oxides (wt.%) of the selected samples representative of distinct groups of CDW materials. Concrete are is in CaO and LOI (volatiles) and relatively poor in SiO₂, whereas bricks, tiles, roof tiles and perforated bricks are rich in SiO₂

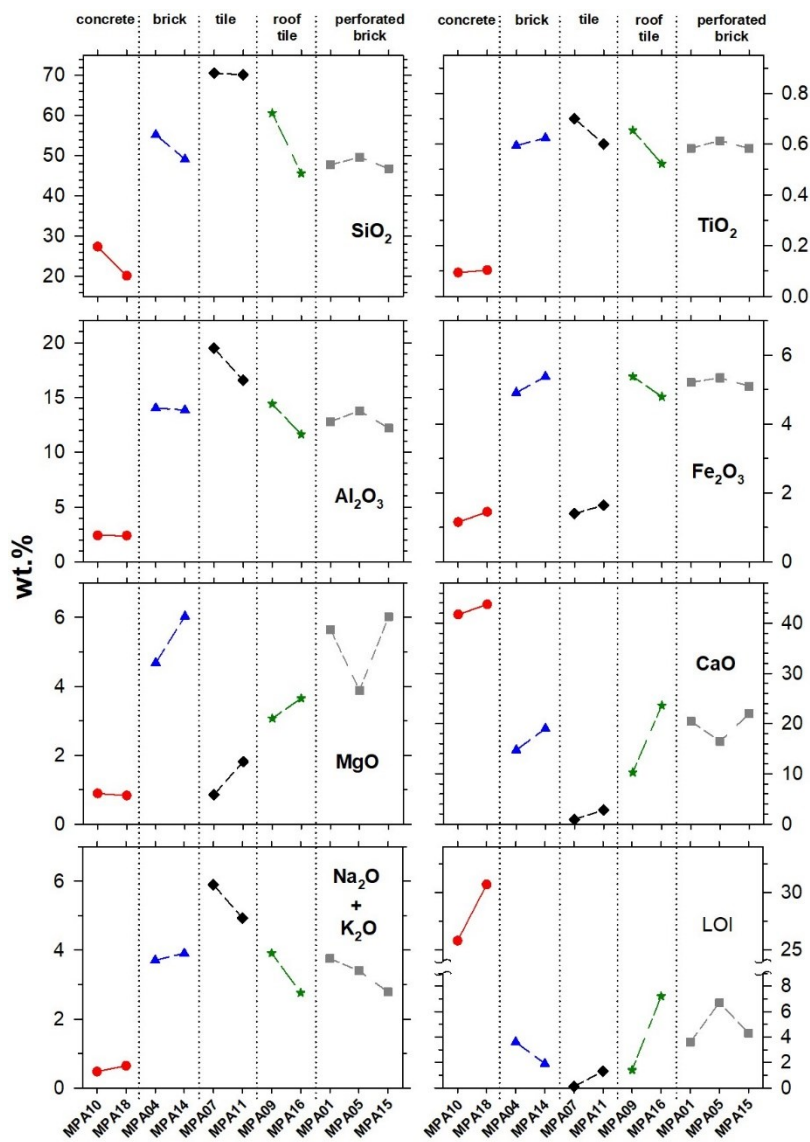


Fig. 4. Scatter plot of the results obtained from XRF analyses. Contents of major oxides among samples and groups. Some elements are plotted together as a function of their chemical characteristics.

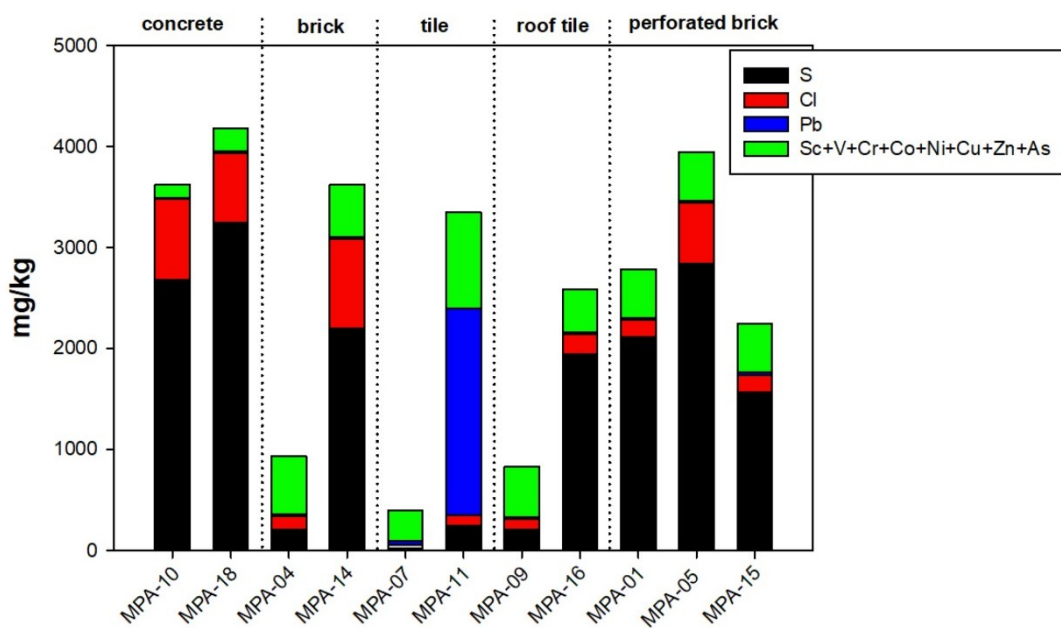


Fig. 5. Comparison of the abundance of minor and trace elements of samples and groups to highlight the most significant differences. Some minor and trace elements are plotted together as a function of their chemical characteristics.

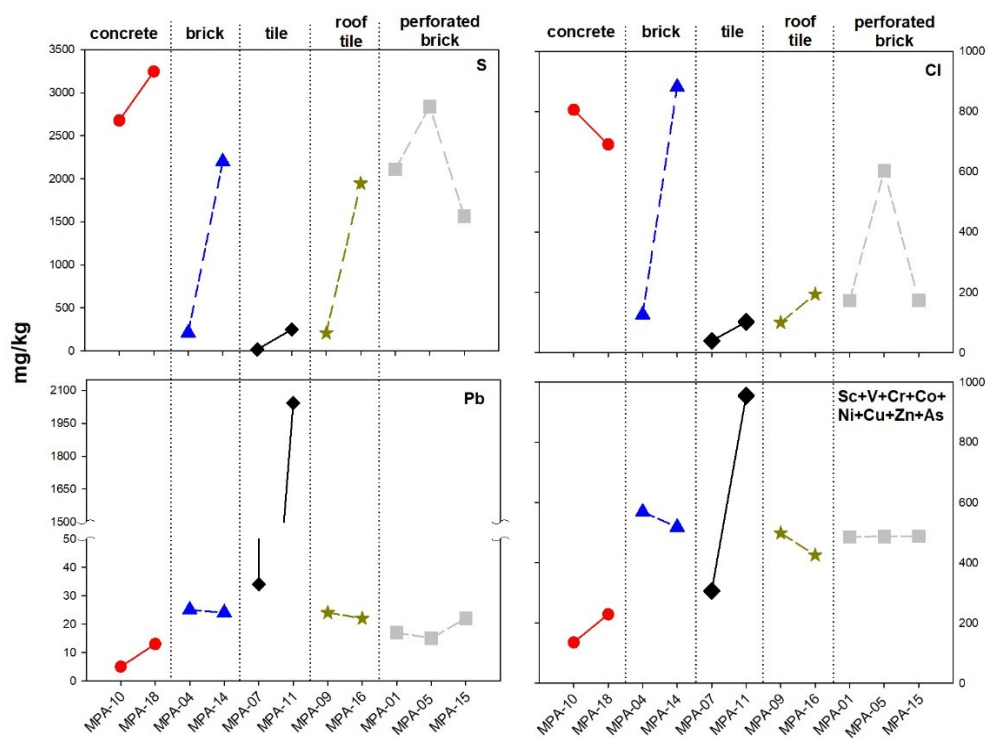


Fig. 6. Contents of minor and trace elements among samples and groups. Some elements are plotted together as a function of their chemical characteristics.

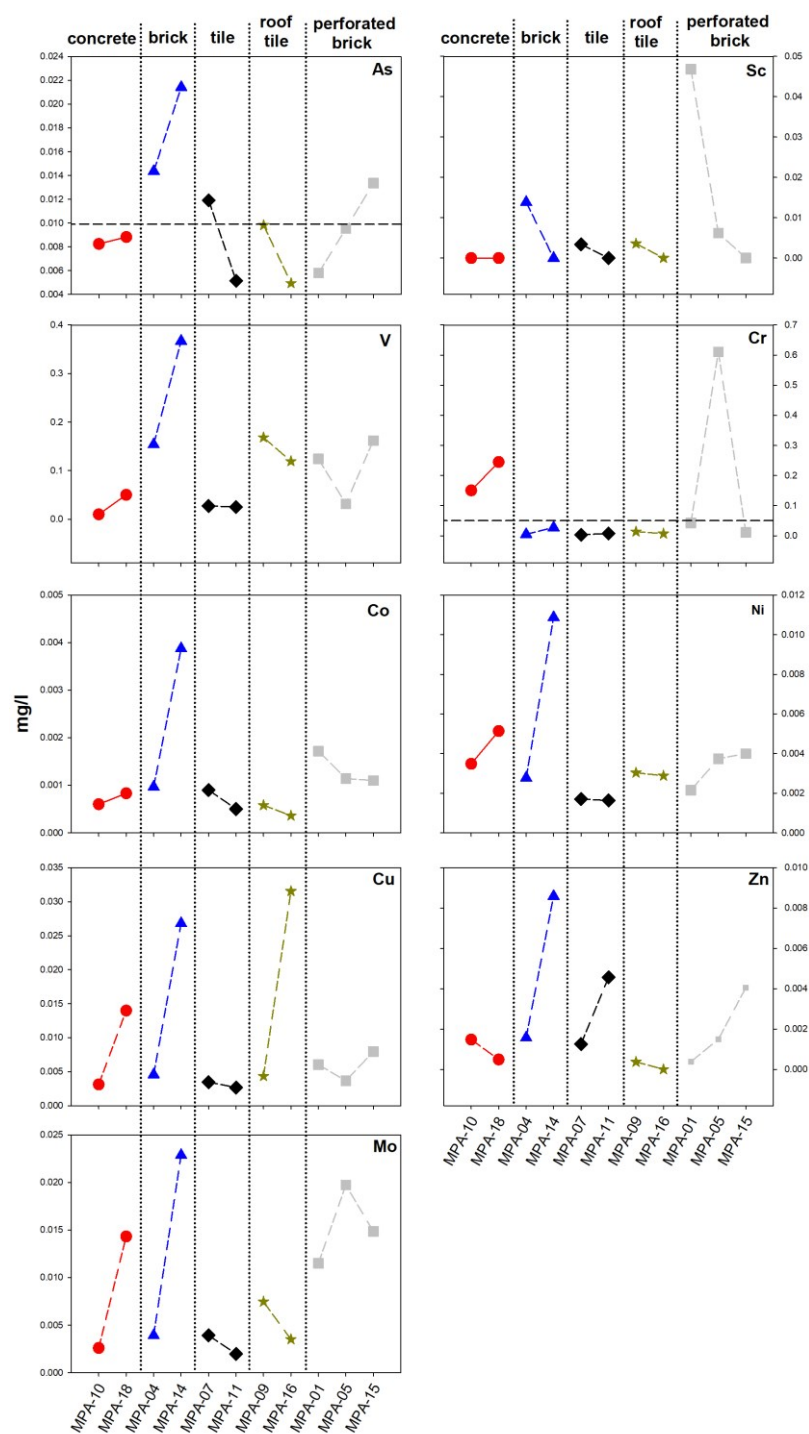


Fig. 7. Contents of As, Sc, V, Cr, Co, Ni, Cu, Zn and Mo in leachates. The black dotted line indicates the Italian Threshold Values of Heavy Metals (TVHM) (see Table S5).

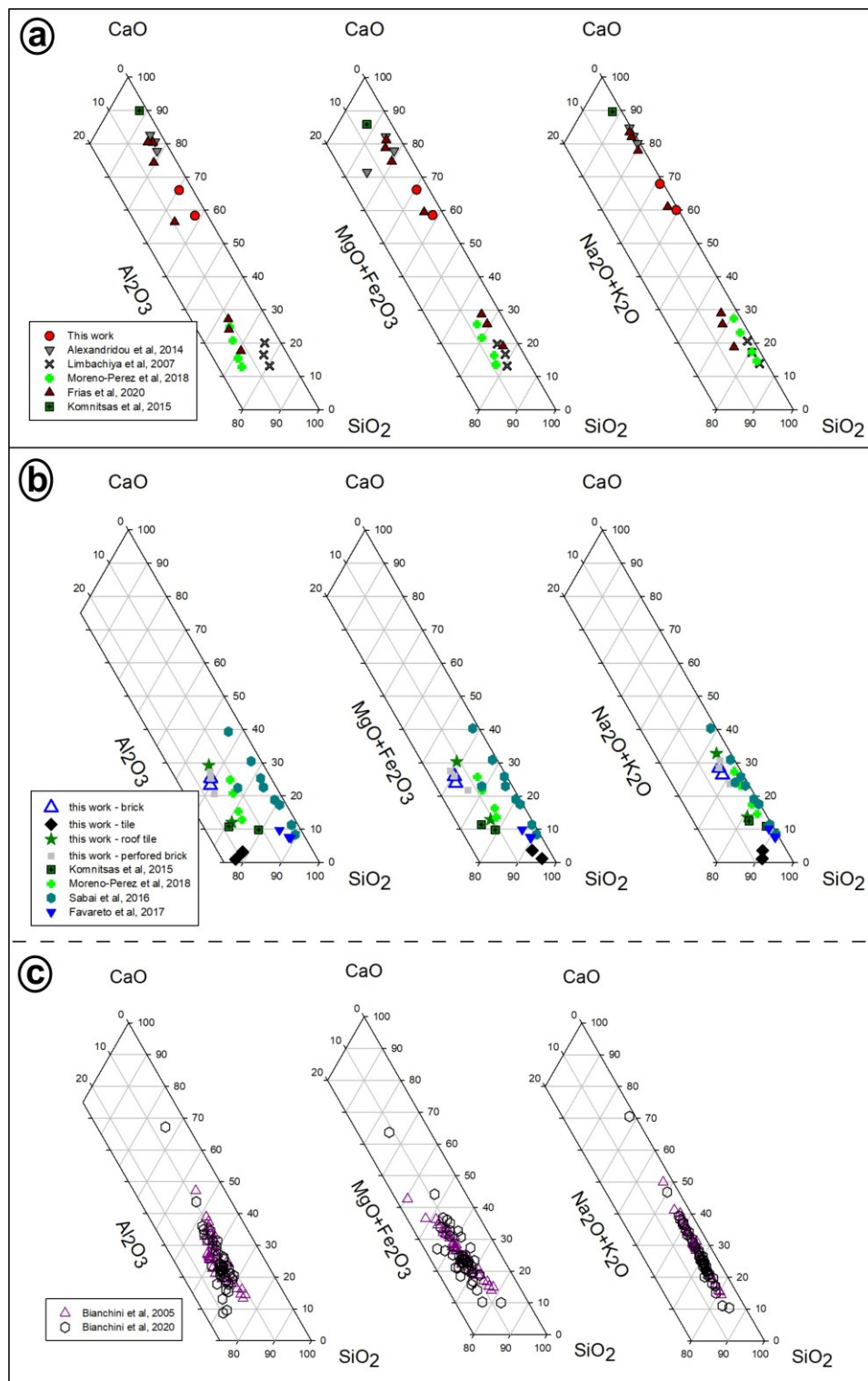


Fig. 8. Major chemical oxides of CDW from different provenance worldwide. a) CDW made of concrete; b-c) CDW made of masonry and ceramics. These data are reported in Table S3.

674
675
676
677
678
679
680
681
682
683
684
685
686
687
688
689
690
691
692
693
694
695
696
697
698
699

Supplementary figures

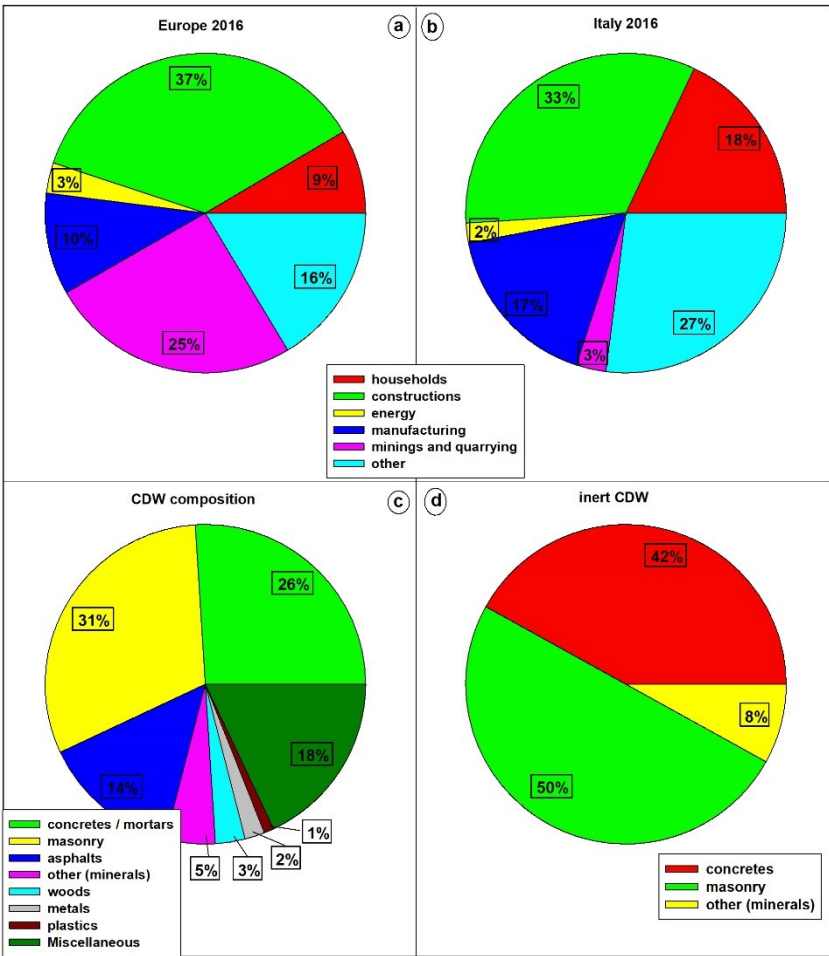


Fig. S1. Shows the amount (wt. %) of wastes in Europe and Italy (a and b) as a function of activity (http://ec.europa.eu/eurostat/statistics-explained/index.php/Waste_statistics); types of material in a general CDW (c) and types of material in the ceramic-like and inert CDW fraction (d) in the EU (or similarly in Italy). “Masonry” includes bricks and perforated bricks, “other mineral” refers to tiles, roof tiles and stone, while “miscellaneous” considers textiles, RAEE, glass, dredging materials and others.

734
735
736
737
738
739
740
741
742
743
744
745
746
747
748
749
750
751
752
753
754
755
756
757
758
759
760
761
762
763
764
765
766
767

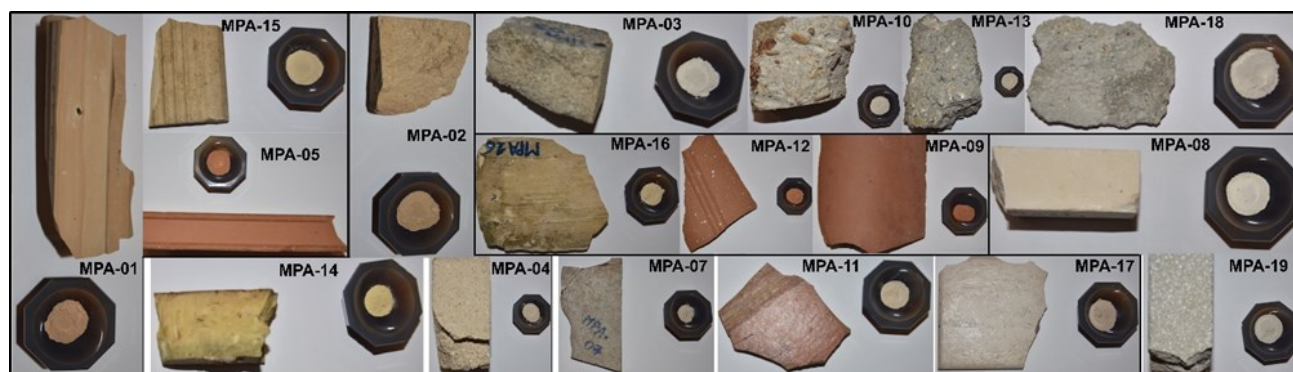


Fig. S2. Mesoscopic (bulk and as-received) samples of CDW collected in the Abruzzo region (Central Italy), and resulting powder samples

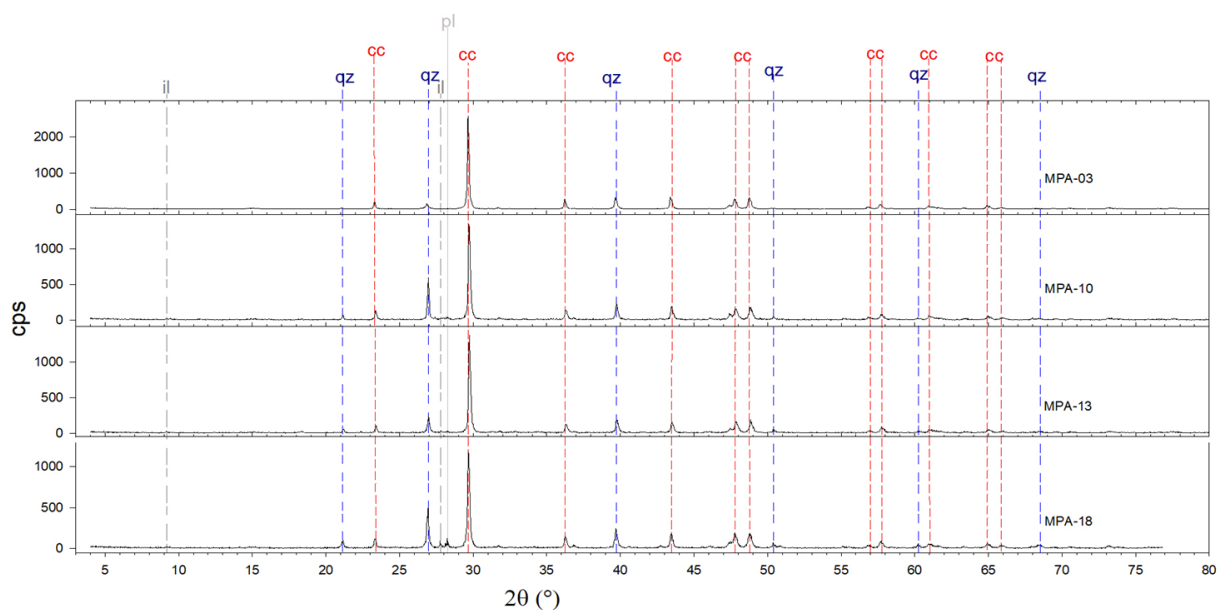


Fig. S3a. Stacked XRPD patterns of concrete (Table 1S); the vertical lines correspond to Bragg reflections of crystalline standards of the ICSD database; cps indicates count per second; calcite (cc), quartz (qz), illite (il), plagioclase (pl).

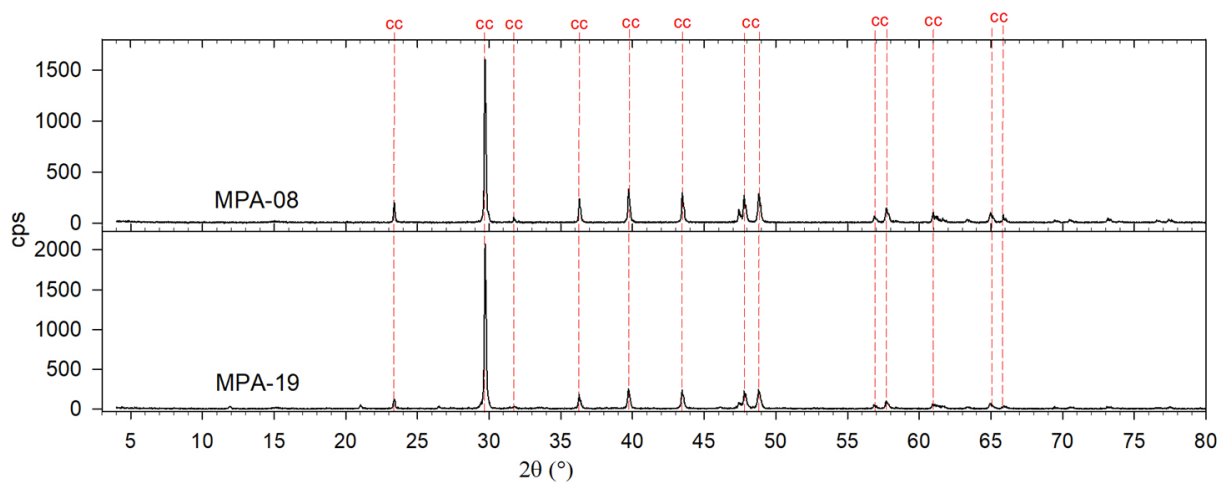


Fig. S3b. Stacked XRPD patterns of natural stone (Table 1S); the vertical lines correspond to Bragg reflections of crystalline standards of the ICSD database; cps indicates count per second; calcite (cc).

Fig. S3c. Stacked XRPD patterns of bricks (Table 1S); the vertical lines correspond to Bragg reflections of crystalline standards of the ICSD database; cps indicates count per second; calcite (cc), quartz (qz), plagioclase (pl), cristobalite (cri), k-feldspar (kf), clinopyroxene (cpx), mullite (mu), melilite (me).

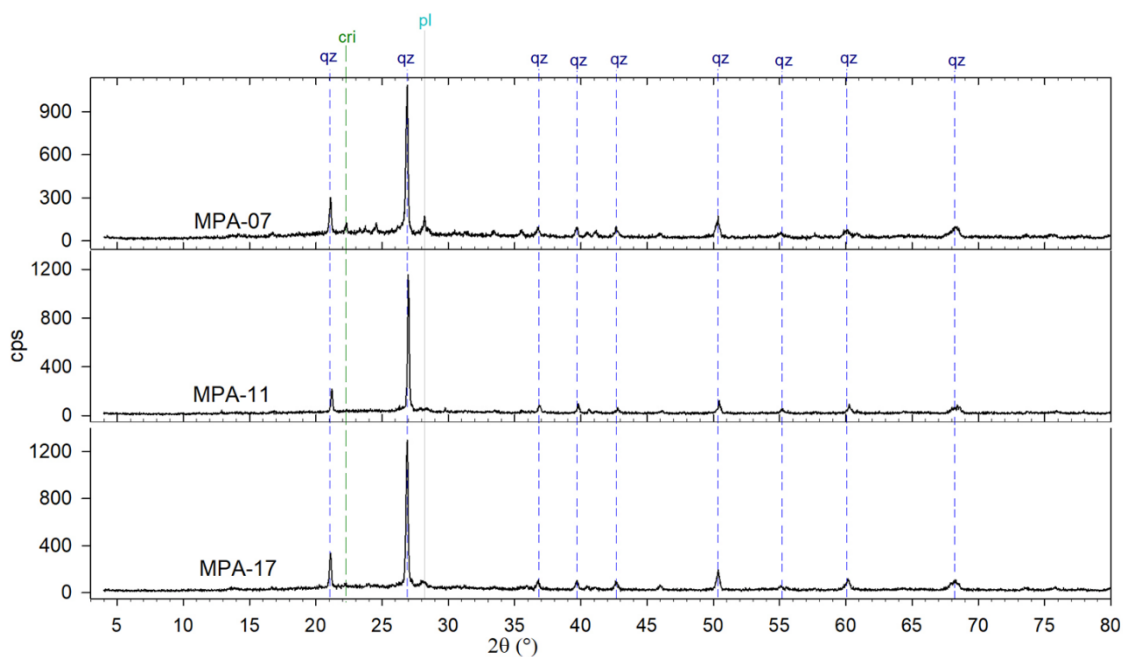


Fig. S3d. Stacked XRPD patterns of tiles (Table 1S); the vertical lines correspond to Bragg reflections of crystalline standards of the ICSD database; cps indicates count per second; quartz (qz), plagioclase (pl), cristobalite (cri).

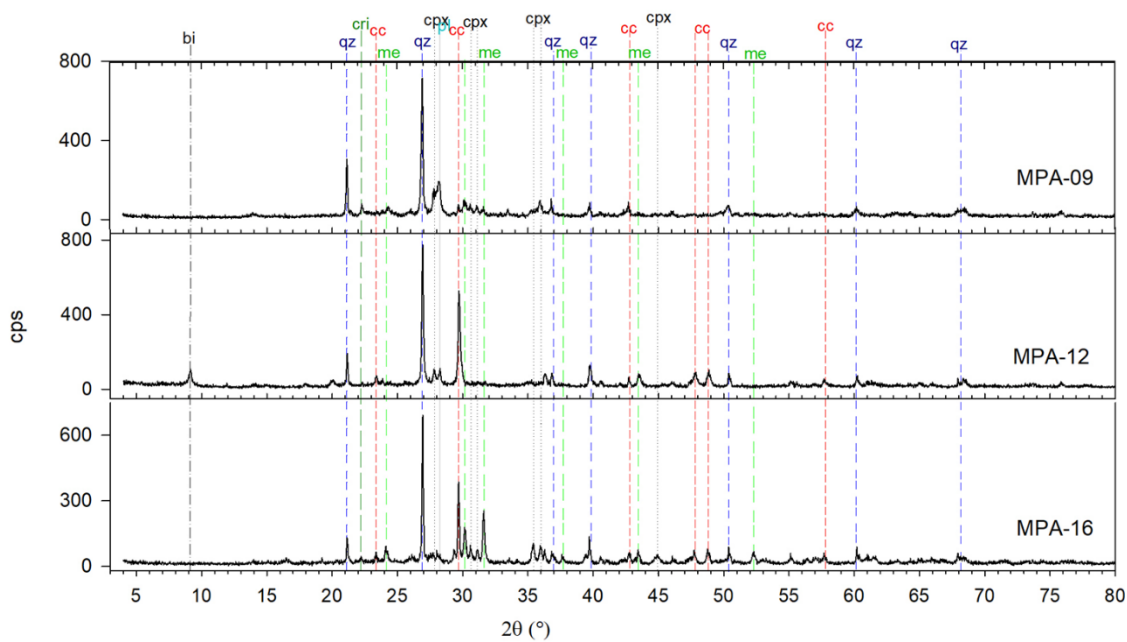


Fig. S3e. Stacked XRPD patterns of roof tiles (Table 1S); the vertical lines correspond to Bragg reflections of crystalline standards of the ICSD database; cps indicates count per second; calcite (cc), quartz (qz), plagioclase (pl), cristobalite (cri), clinopyroxene (cpx), melilite (me), biotite (bi).

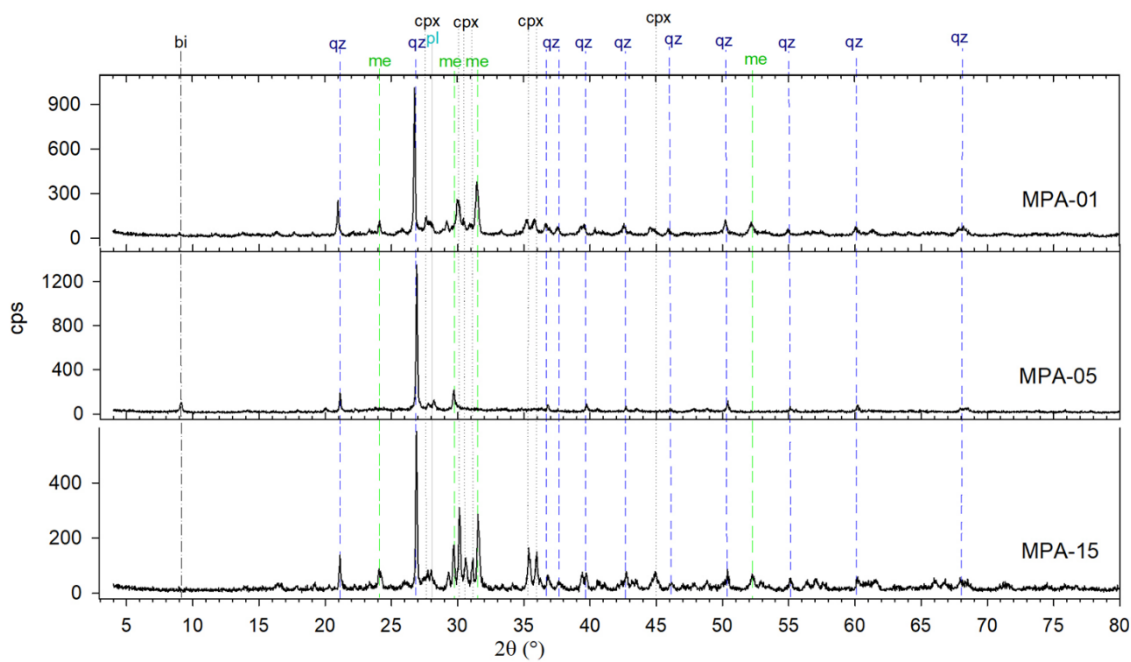


Fig. S3f. Stacked XRPD patterns of performed bricks (Table 1S); the vertical lines correspond to Bragg reflections of crystalline standards of the ICSD database; cps indicates count per second; calcite (cc), quartz (qz), plagioclase (pl), clinopyroxene (cpx), melilite (me), biotite (bi).